

Finite element impact analysis for the design of structurally dissipating rock-shed

Yi Zhang^{1*}, François Toutlemonde² and Philippe Lussou^{2,3}

¹Technical Direction, Spie batignolles TPCI, 11 rue Lazare Hoche,
92774 Boulogne-Billancourt Cedex, France

²Université Paris Est-LCPC (Laboratoire Central des Ponts et Chaussées),
58 bd. Lefebvre, 75732 Paris Cedex 15, France

³Lafarge Centre de Recherche, 95 rue du Montmurier 38070 Saint-Quentin-Fallavier Cedex, France
(Receive January 18, 2008, Accepted February 23, 2009)

Abstract. This paper presents finite element impact analysis for the design of Structurally Dissipating Rock-shed (SDR), an innovative design of reinforced concrete rock-shed. By using an appropriate finite element impact algorithm, the SDR structure is modelled in a simplified but efficient way. The numerical results are firstly verified through comparisons with the results of the experiments recently realized by ESIGEC and TONELLO I.C. It is shown that, using this impact algorithm, it is possible to correctly predict the SDR structural behaviour under different rock-fall impact conditions. Moreover, the numerical results show that the slab centre is the critical impact location for reinforced concrete slab design. The impact analyses have thus been focused on the impacts at the slab centre for the SDR structural optimization. Several series of parametric studies have been carried out with respect to load cases and engineering parameters choices. These numerical results support the robustness of the new SDR concept, and serve to optimize SDR structure and improve its conventional engineering design, especially for ensuring the slab punching shear resistance.

Keywords: structurally dissipating rock-shed; rock-fall impact; finite element impact analysis; structural design; structure sensitivity study; punching shear.

1. Introduction

The protection of civil structures such as railways and roads against rock-fall impacts is one of the major problems of civil engineering in Alpine mountain region. In France, the concept of Structurally Dissipating Rock-shed (SDR) has been invented by Tonello I.C. to optimize structural shape, save construction materials and simplify structural maintenance (IVOR 2001). It is made of a reinforced concrete slab supported by specially designed steel fuse supports (Fig. 1). As opposed to traditional rock-shed (OFR 1998), SDR needs no more the thick absorbing soil cushion over the structure, it uses directly reinforced concrete slab movement and deformation, and fuse supports damage, to dissipate rock block impact energy.

The SDR conventional structural design uses a single-degree-of-freedom mass-spring model. Assuming that neither rebound of rock block nor penetration into R.C. slab occurs during impact, slab is considered to deform in the first vibration mode to dissipate the kinetic energy, and the

* Ph.D., Corresponding author, E-mail: yi_zhang@spiebatignolles.fr

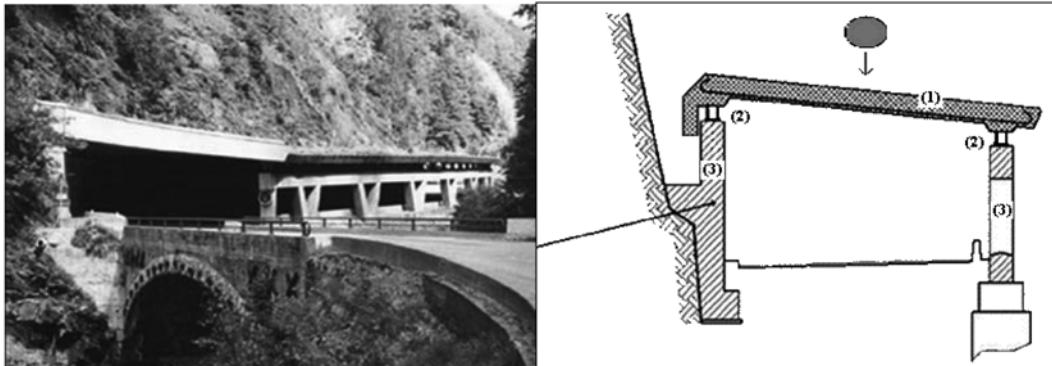


Fig. 1 Photo of SDR structure “les Essariaux” and its schematic section (IVOR 2001): (1) R.C. slab, (2) Fuse supports, (3) Supporting structure

impact force is determined from the impulsion balance with the impact duration equal to a quarter of the structural period. Limits of this approach are discussed in (Lussou and Toutlemonde 2005). Moreover, the experiments carried out by ESIGEC and TONELLO I.C. have proved that this conventional design method correctly accounts for flexure-dominated deformation modes (Delhomme *et al.* 2005). However, since punching shear may be critical, the shear reinforcement classically provided in current R.C. slabs is not sufficient to resist the important punching force. In order to improve this conventional engineering design, the impact force should be precisely evaluated. According to a rigorous structural modelling and finite element impact analysis of SDR structure, the numerical results are found to be very sensitive to several contact parameters like impact angle and friction coefficients (Berthet-Rambaud *et al.* 2003), and the complexity of impact modelling makes the model parameters calibration difficult.

Therefore the presented impact analysis has focused on simulating SDR structural response under rock-fall impacts in a simplified but efficient way to find out the ultimate limit states for SDR structure design, with appropriate engineering safety margin, and using only a few parameters directly calibrated from experiments. With this aim in view, in this paper, the appropriate Three-Dimensional finite element impact analyses are presented. They are aimed to simulate SDR structural behaviour under different rock-fall impact conditions.

2. Development of an appropriate finite element impact algorithm

2.1. Impact analysis hypotheses

As SDR structure is directly submitted to the transient load during rock-fall impacts, an appropriate impact analysis is thus necessary to study the interaction between rock block and SDR structure, in which materials dynamic behaviour also needs to be taken into account. A simplified impact algorithm has been developed under the small deformation hypothesis, which is the case for concrete structures before global failure. It has then been implemented in the CESAR-LCPC finite element code (Humbert *et al.* 2005). Based on the previous developments aimed at designing waste containers in case of fall (Sercombe 1997, Toutlemonde *et al.* 1999, Lussou *et al.* 2005), these new developments, detailed in (Zhang 2006), provide an analysis tool for SDR structure:

- by keeping a simplified geometrical approach, the block is considered as rigid with a locally spherical shape;
- by keeping a simplified impact approach, only the perpendicular impacts without friction have been taken into account.

These hypotheses have been chosen to identify the ultimate limit states for SDR structure design. They allow considering the critical impact situations with limited parameters and give the numerical results a non excessive safety margin. At first, the block is assumed to be rigid. This avoids the uncertainties of block shape variation and simplifies contacting nodes search, since the impacting block is dealt with as a geometrical condition imposed on the structure. It also overestimates loading of the structure during impact analysis because of neglecting the block deformation energy dissipation, which is conservative for engineering design. Furthermore, since the block is assumed to impact perpendicularly the structure, no frictional effects are considered in the impact algorithm. This avoids the heavy calibration of impact parameters and limits the impact parameters number. It also leads to overestimate the load on the structure during impact analysis by neglecting the frictional energy dissipation, which is conservative for engineering design.

2.2. Material model

Concrete is considered as a rate sensitive material, the experimental results show that its mechanical characteristics (strength, elastic modulus) increase when strain rate increases (CEB 1988). In the strain rate range from 10^{-6} to 10 s^{-1} , its strength and elastic modulus increase almost linearly versus strain rate in a semi-logarithmic scale. In this strain rate range, this rate-dependance can be explained by viscous effects due to the presence of liquid (free water) within the nanopores of concrete (Harsh *et al.* 1990, Rossi 1997). Moreover, in this strain rate range, rate effects are not related to inertia of structure parts moving apart due to cracking, as it is the case for strain rates greater than 10 s^{-1} .

Based on the non-plastic hardening theories of Coussy (Coussy 1995) and Ulm (Ulm and Coussy 2001), Sercombe has developed an elastoplastic damage model with viscous hardening (Sercombe *et al.* 1998) to model concrete dynamic behaviour for strain rates less than 10 s^{-1} , which is the case of numerous dynamic loading conditions in civil engineering, such as the rock-fall impacts. So, it has been adopted here for the concrete model.

As for the steel model, steel bars are less sensitive to the strain rate in the strain rate range from 10^{-6} to 10 s^{-1} , their behaviour can be modelled using an elastoplasticity model with plastic hardening without dependence to the strain rate. A Von Mises model is adopted here for steel reinforcing bars and steel fuse supports.

2.3. Finite element impact algorithm

The Newmark method is used for the integration of dynamic equilibrium equation. In its incremental scheme, a contact treatment is added, which allows to find out nodes in contact and to calculate the structural stresses and the impact force by the nodal forces integration.

A trial and error procedure is adopted to find out the nodes in contact. It consists of a trial selection and an error elimination: a potentially new contacting node is defined to be a contact node if its distance to the target node (or a similar geometrical condition) is smaller than the control distance; then the contact force in this node is calculated, which should not be greater than zero

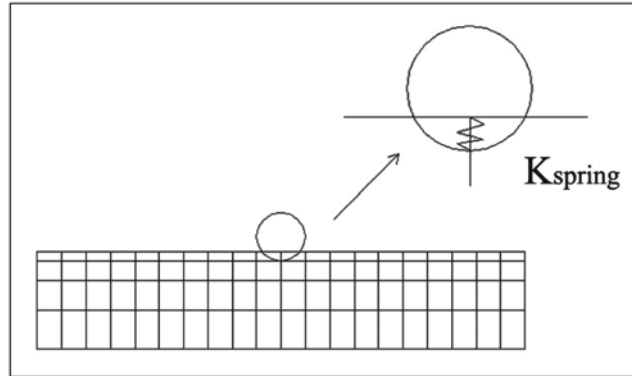


Fig. 2 Penalty method scheme (spherical impacting block case)

according to the Kuhn-Tucker conditions of a unilateral contact problem. A trial node that does not satisfy this mechanical contact condition will be referred to as an error node and be considered as not in contact.

After this trial and error detection, if the nodes are tested to be in contact, the penalty method is used to prevent inter-penetration between the two contacting objects and calculate the contact force. It has been chosen for its robustness and easiness to be implemented in a finite element code. Physically, this method means placing additional interface springs between contacting surfaces, in this way the contact force is proportional to the penetration distance by introducing a penalty parameter (Fig. 2).

The Newmark method with added contact treatment ensures the compatibility of displacements between two impacting bodies. The velocity and acceleration compatibilities are ensured by imposing the block velocity and acceleration to the structure nodes in contact with the block. Since numerical instabilities can be generated in the Newmark integration scheme due to the contact surface changes, we have withdrawn the iteration for the resolution of the equilibrium equation. As a consequence, the time step should be chosen small enough to reduce the residual.

2.4. Flowchart of the developed impact algorithm

Fig. 3 illustrates the flowchart of the developed impact algorithm implemented in the CESAR-LCPC F.E. code (thick: new developments). This impact algorithm has been validated with three reference cases of elastic impact computations: two impacting bars, a sphere impacting a slab and a sphere impacting a mass. The numerical results are found to be in good agreement with the analytical results. This impact algorithm has then been used for the plastic impact computation in the case of a sphere impacting a mass, the numerical results are found to be reasonable although no analytical results are available (Zhang 2006).

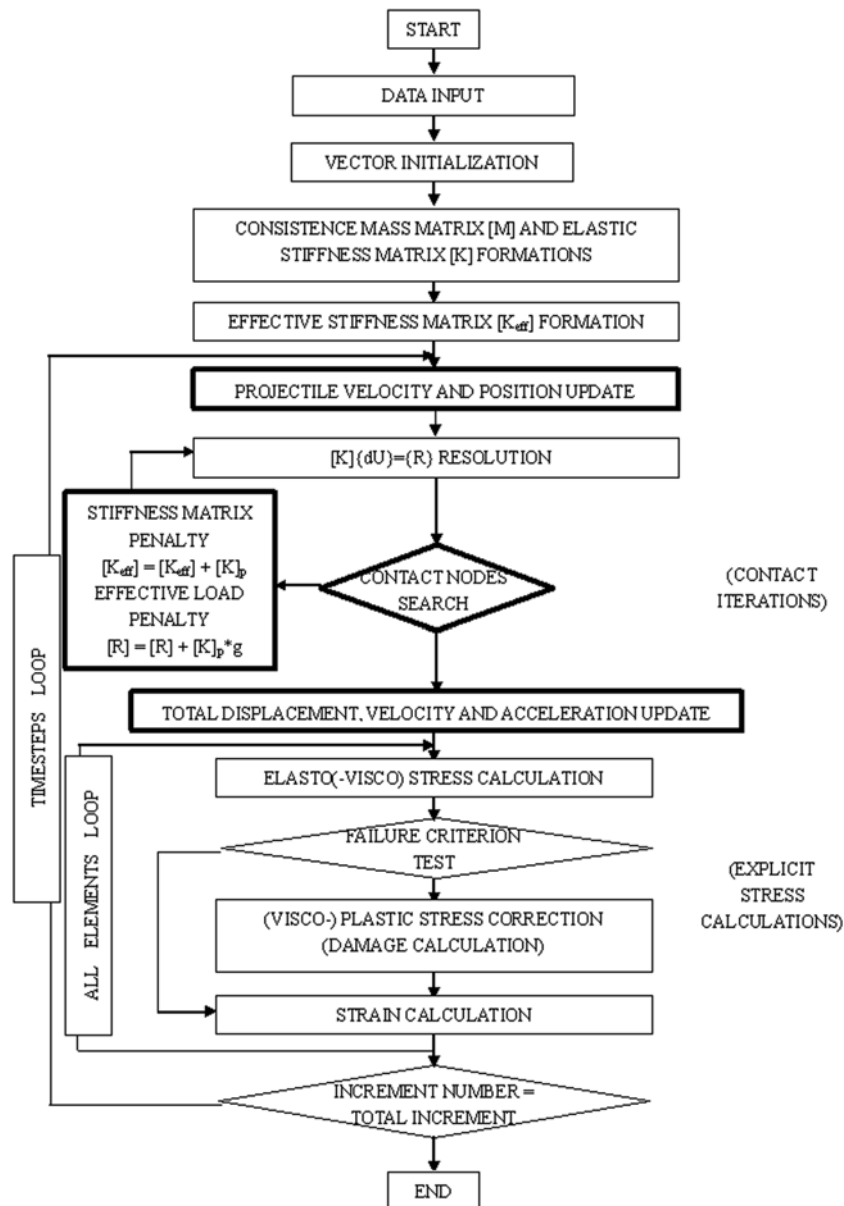


Fig. 3 Flowchart of the developed impact algorithm

3. Verification of the developed impact algorithm

3.1. Description of the experiments

A series of experiments on a 1/3 scaled SDR structure have been carried out by ESIGEC and TONELLO I.C. (Delhomme *et al.* 2005). This structure consists of a horizontal reinforced concrete slab resting on 2 lines of 11 steel fuse supports. Their base is considered to be rigid. Three zones of

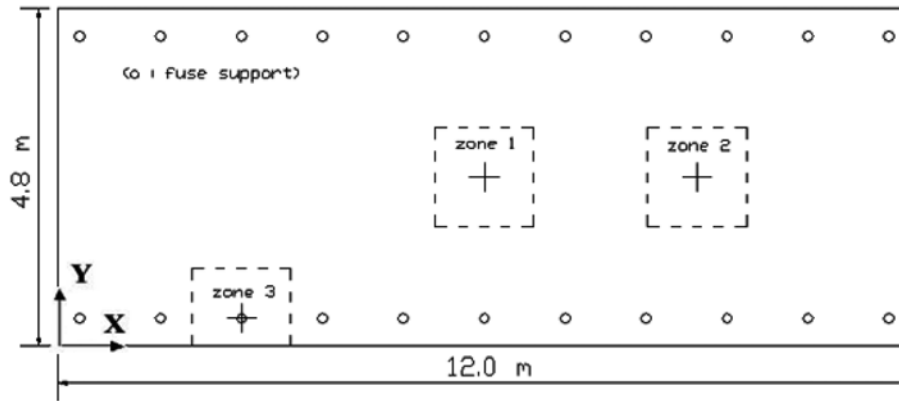


Fig. 4 Three impact zones on the model slab

the slab have been impacted by blocks of different shapes dropped from different heights: zone 1 is at the centre of the slab, zone 2 is on the side span of the slab, and zone 3 is on the edge of the slab above a fuse support (Fig. 4).

The dimension of the slab is 12 m*4.8 m*0.28 m (length*width*thickness). It is made of 30 MPa-concrete. All reinforcing bars have a 500 MPa-yield stress. The distance between fuse supports is 1.14 m, each fuse support is made up of a steel tube (TUE 220A/height: 100 mm, diameter: 70 mm, thickness: 2.9 mm) welded onto two plates (thickness: 8 mm) and supported by a neoprene layer (surface: 100 mm*100 mm, thickness: 10 mm).

The six impact tests presented in (Delhomme *et al.* 2005) have been simulated with the developed impact algorithm. These reference tests correspond to falling block energies under which the slab: remains undamaged (Serviceability Limit State: SLS); endures limited damage with possibly moderate steel reinforcement yielding (“Ultimate” Limit State: ULS); is significantly damaged but without important concrete block losses and maintains overall stability (“Post-Ultimate” Limit State: PULS). This non-standard definition of limit states is of interest for structures critically dimensioned by accidental loadings, where the stage of limited damage possibly easy to be repaired should find a valuable domain of application in optimized design. The details of tests carried out are listed in Table 1.

Table 1. Simulated impact tests

Impact test	Impact zone	Block mass (kg)	Block shape	Drop height (m)	Initial impact velocity (m/s)	Impact energy (kJ)
T1	Zone 1 (X=6.0 m, Y=2.4 m)	450	cube	15	17.3	67 (SLS)
T2	Zone 2 (X=9.0 m, Y=2.6 m)	450	cube	30	24.5	135 (ULS)
T3	Zone 3 (X=2.4 m, Y=0.8 m)	450	cube	30	24.5	135 (ULS)
T4	Zone 2 (Repaired after T2) (X=9.0 m, Y=2.6 m)	470	cube	30	24.5	141 (ULS)
T5	Zone 1 (Damaged by T1) (X=6.0 m, Y=2.6 m)	455	cube	30	24.5	137 (ULS)
T6	Zone 2 (Damaged by T4) (X=9.1 m, Y=2.7 m)	810	diamond-cut	37	27.2	300 (PULS)

3.2. Finite element model

As for the finite element model, since the different impact zones have to be taken into account, the whole structure is modelled. The reinforced concrete slab is modelled as a concrete solid volume (volume elements) connected to a steel bars frame (nonlinear beam elements) at nodes. The corresponding elements are assumed in perfect contact. The fuse supports are modelled with nonlinear beam elements, a Von Mises with hardening model is used for the fuse supports modelling. The neoprene layers under fuse supports are modelled with elastic beam elements for sake of simplicity. Fig. 5 illustrates the Three-Dimensional finite element mesh of the tested SDR structure. There are 4 layers (z direction) in the slab, one for the concrete cover layer on each side, 0.04 m thick, and two in-between 0.1 m thick. In each layer, there are 120 elements in the longitudinal direction (x) and 41 elements in the transverse direction (y). In total, the mesh consists of about 19000 8-noded volume elements and about 25000 2-noded beam elements. The mesh is refined around the impact points.

At the beginning of impact, the rigid spherical block is in contact with the slab at the impact location with an initial velocity perpendicular to the surface (Fig. 6). As for the boundary conditions, the structure is simply supported by applied prescribed displacements ($u=0$ in x direction, $v=0$ in y direction and $w=0$ in z direction) at the base of the beam elements representing the supports.

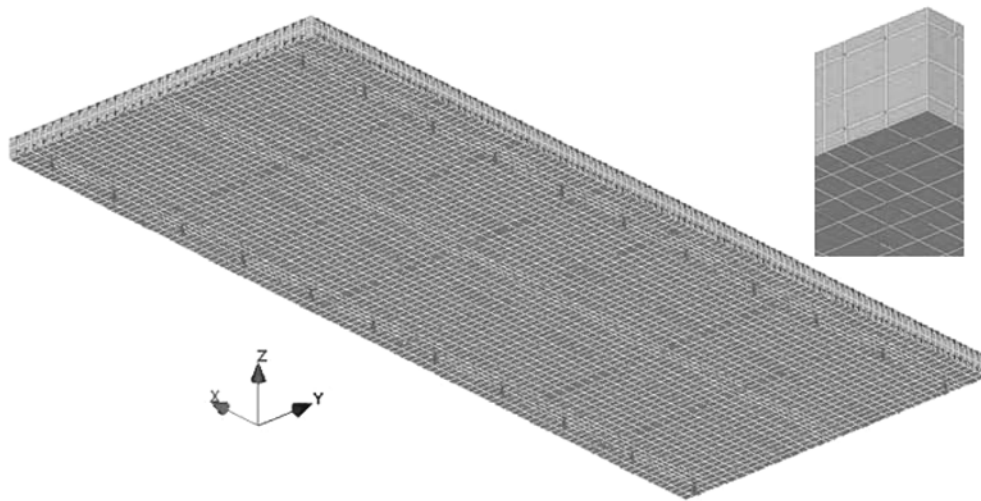


Fig. 5 Three-Dimensional finite element mesh of the tested SDR structure with fuse support modelling details

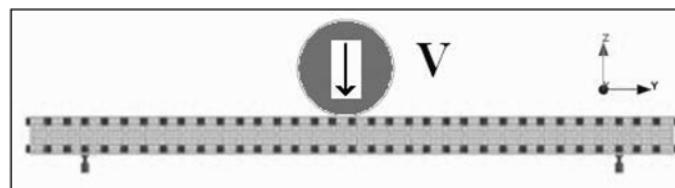


Fig. 6 Initial impact position (T1)

3.3. Input parameters values

The material properties used for the computations are listed in Tables 2, 3 and 4. For concrete, besides its physical and static mechanical properties (specific gravity, Poisson's ratio, tensile strength, uniaxial and biaxial compressive strength, triaxial strength and elastic modulus), the application of the elastoplastic damage model with viscous hardening requires the determination of two other parameters: α , the absolute increase in tensile strength per logarithmic unit of loading rate; E_{lim}^{dyn} , the asymptotic dynamic modulus, extrapolated to a uniaxial tensile test at a loading rate of 100 GPa/s. The values of these two parameters are obtained from the existing test results (Toutlemonde and Rossi 1995) and calibration procedure is detailed in (Sercombe *et al.* 1998). Furthermore, the damage of concrete is considered by assuming an exponential decay of the elastic modulus: $E(\chi)=E.exp(-r\langle\chi\rangle)$ with $r=150$, in which only concrete plastic dilatation ($\chi>0$) is considered to cause the elastic modulus change. This damage evolution allows the concrete crushing and energy absorption near impact point to be modelled during impact. For the tests T5 and T6, as the slab has already been damaged by the previous impact test, a predefined damage is introduced in the impact zone by a damaged modulus $E=14$ GPa for T5 and $E=8$ GPa for T6, these values are calculated according to the slab damage degree after the previous impact.

Table 2. Concrete properties used for impact analyses

Elasticity	specific gravity (ρ)	2500 (kg/m ³)
	static elastic modulus (E)	30 [32]* (GPa)
	Poisson's ratio (ν)	0.2
Plasticity	uniaxial compressive strength (σ_c)	30 [35]* (MPa)
	uniaxial tensile strength (σ_t)	2.4 [2.9]* (MPa)
	biaxial compressive strength (σ_{bc})	33 [39]* (MPa)
	triaxial strength (τ_{ult} , σ_{ult} , θ)	($-3.9\sigma_c$, $2.44\sigma_c$, 0°)
Viscosity	asymptotic dynamic modulus (E_{lim}^{dyn})	37 (GPa)
	absolute increase in tensile strength (α)	0.8 (MPa/log. unit)
Damage	exponential coefficient (r)	150

*: concrete properties in repaired zone 2.

Table 3. Steel properties used for impact analyses

Elasticity	specific gravity (ρ)	7800 (kg/m ³)
	elastic modulus (E)	210 (GPa)
	Poisson's ratio (ν)	0.3
Plasticity	simple shear strength (τ)	289 (MPa)
	hardening modulus (H)	1 (GPa)

Table 4. Neoprene properties used for impact analyses

Elasticity	specific gravity (ρ)	1500 (kg/m ³)
	elastic modulus (E)	85.8 (MPa)
	Poisson's ratio (ν)	0.49

The time step is chosen as 1.5×10^{-5} s, which is small enough with respect to the Courant's condition. The penalty parameter is chosen as 1×10^{15} N/m, tests show that numerical results are not excessively sensitive to penalty parameter value of this order (Zhang 2006). No damping is considered in the impact analysis in order to find out the ultimate limit states for SDR structure design.

3.4. Numerical results vs. experimental results

The impact analysis results provide detailed information about the SDR structural response under the impact tests such as impact force, structural displacements, stresses and strains in elements. This information is classified here according to 3 main aspects:

- Dynamic interaction between impacting structures: impact force;
- Structural global results: displacements and support reactions;
- Structural local results: axial stresses and strains in steel bars, stresses and strains in concrete.

3.4.1. Dynamic interaction-impact force

The numerical results of impact force (amplitude, duration and impulsion) corresponding to the 6 tests are listed in Table 5 in comparison with the available experimental results, which have been measured by the accelerometers (Delhomme *et al.* 2005). As for the difficulties, few measured impact forces are available. For the slab punching resistance verification, the numerical impact force values are found to be conservative as a result of the simplified hypotheses. As an example, experimentally, two impacts occurred during the test T4. Numerically, only one impact has been simulated. As Fig. 7 illustrates, the numerically estimated impact force peak in the test T4 is conservative, and the combination of the two measured impulsions is close to the numerical one. Moreover, the numerical results also show that impact force duration is much less than one quarter of the structural period (about 60 milliseconds) under a ULS impacting energy, which was assumed as the impact duration in the SDR conventional structural design method. The design impact force determined from the impulsion balance, due to impact duration overestimation, is thus underestimated, and this should be improved in the SDR structural design studies.

Table 5. Numerical results of impact force

Impact test	Experimental results			Numerical results		
	Impact force amplitude (MN)	Impact duration (ms)	Impulsion (kN.s)	Impact force amplitude (MN)	Impact duration (ms)	Impulsion (kN.s)
T1	---	---	---	4.7	4.0	9.2
T2	---	---	---	5.3	5.5	13.2
T3	---	---	---	5.0	5.3	12.4
T4	1 st impact : 2.7 2 nd impact : 3.0	1 st impact : 3.4 2 nd impact : 3.2	1 st impact : 4.8 2 nd impact : 6.7	5.8	5.2	13.9
T5	---	---	---	5.8	4.9	13.4
T6	1 st impact : 4.9 2 nd impact : ---*	1 st impact : 4.0 2 nd impact : ---*	1 st impact : 21.2 2 nd impact : ---*	6.1	10.1	25.2

*: no measured result

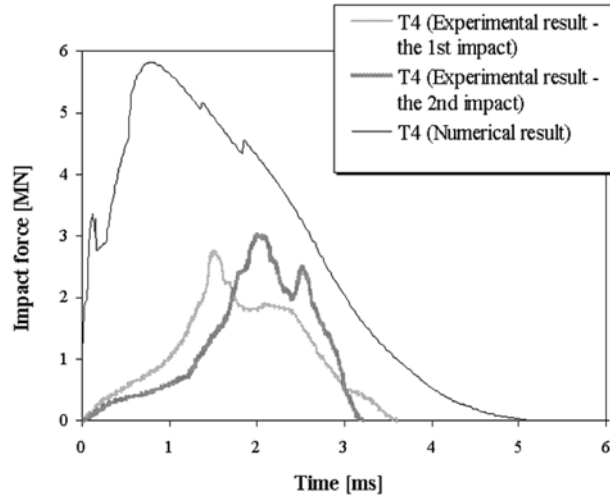


Fig. 7 Comparison of the impact forces (T4)

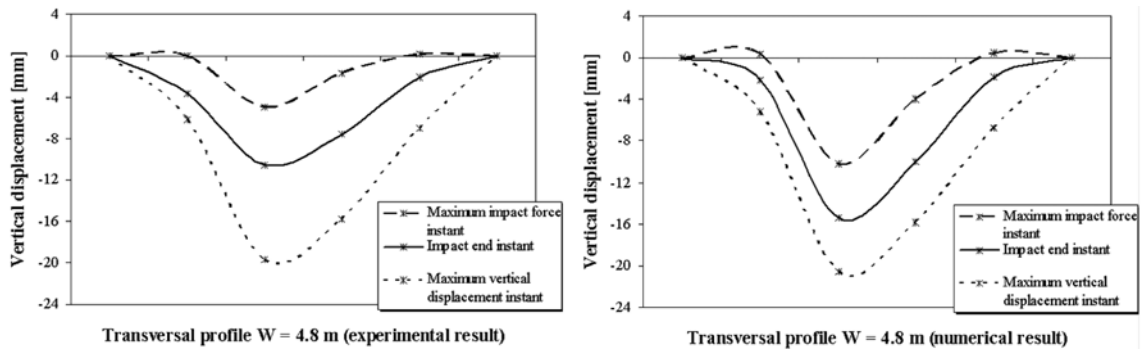


Fig. 8 Deformed transversal profile (vertical displacements) in the test T4

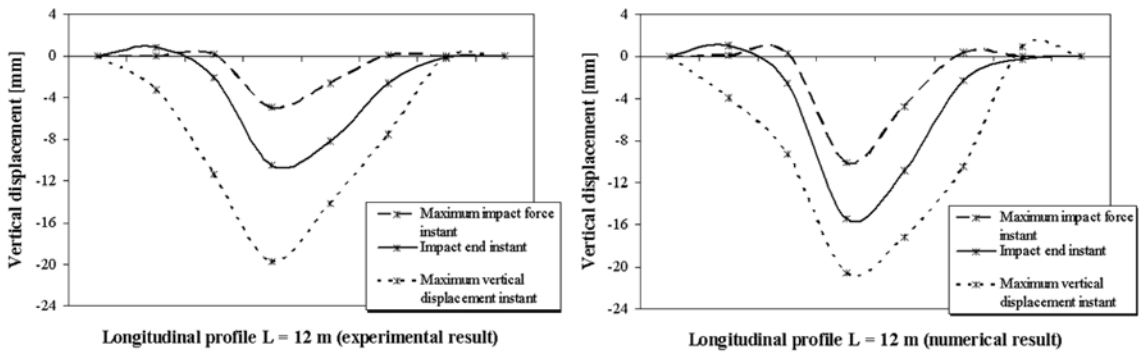


Fig. 9 Deformed longitudinal profile (vertical displacements) in the test T4

3.4.2. Structural global results

Details are given for the vertical structural displacements. For the impacts in zone 1 and zone 2, the maximum takes place in the slab mid-span zone. Fig. 8 and Fig. 9 show the evolution of the deformed profile of the transversal and longitudinal sections respectively. Three representative times

are considered: the time of the maximum impact force ($t \approx 2$ ms); the time corresponding to the end of impact ($t \approx 5$ ms) and the time of the maximum vertical displacement ($t \approx 12$ ms). It is found that, after the short impact duration, during which the impulsion is given to the structure, the slab goes on moving down till it reaches the maximum vertical displacement at about one quarter of the structural fundamental period. For the impact in zone 3, the maximum vertical displacement takes place at the fuse support location.

Concerning support reactions, the experimental observations show that the impacts with ULS energy in zone 1 and zone 2 have not caused any irreversible damage in the fuse supports, and the impacts with ULS energy in zone 3 have led to the buckling of three fuse supports near the impact point. According to the numerical results, an impact with SLS energy in the slab mid-span does not cause damage in the fuse supports, and an impact with ULS energy in the slab mid-span causes slight damage in the fuse supports, the maximum irreversible displacement is about 2 mm, corresponding to a dissipated energy of 0.6 kJ. When an impact with ULS energy occurs above the fuse supports, the maximum irreversible displacement is about 23 mm, corresponding to a dissipated energy of 7 kJ, which indicates a heavy damage of fuse support.

In fact, during impact, the kinetic energy of falling block is partially converted into the block rebound and the slab vibration, the other part of initial impact energy is dissipated by the damage of

Table 6. Structural global results

Impact test	Maximum vertical displacement		Fuse supports yielding	
	Experimental results (mm)	Numerical results (mm)	Experimental results	Numerical results (irreversible displacement)
T1	-14.5	-16.7	no fuse support yielding	no fuse supports yielding
T2	-22.5	-25.0	no fuse support yielding	4 fuse supports limited yielding (2 mm)
T3	-21.5	-22.6	3 fuse supports yielding	3 fuse supports yielding (22.6 mm)
T4	-19.7	-22.4	no fuse support yielding	4 fuse supports limited yielding (2.5 mm)
T5	-23.2	-27.3	no fuse support yielding	6 fuse supports limited yielding (2 mm)
T6	---*	-50.3**	8 fuse supports yielding	8 fuse supports yielding (16.5 mm)

*no measured result due to concrete ejection

**constitutive behaviour assumptions are no more valid (exceeded criterion)

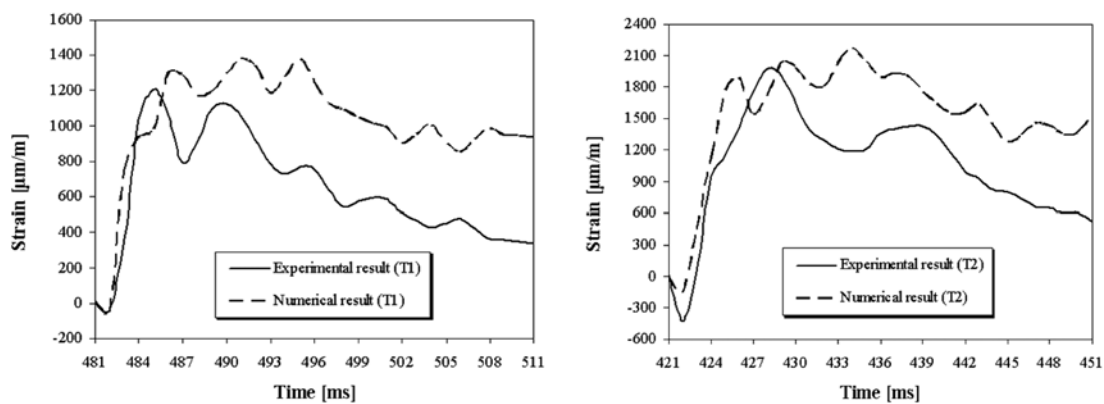


Fig. 10 Strain of flexural reinforcement in the tests T1 and T2

the block, the slab and the fuse supports (Delhomme *et al.* 2005).

Comparison of the measured and calculated maximum vertical displacements and fuse supports yielding is given in Table 6.

3.4.3. Structural local results

In the test T1, the maximum measured strain of flexural reinforcement is 1200 $\mu\text{m}/\text{m}$, and the corresponding numerical strain is 1400 $\mu\text{m}/\text{m}$, about 15% higher. In the test T2, the maximum measured strain of flexural reinforcement is 1980 $\mu\text{m}/\text{m}$, and the corresponding numerical strain is 2170 $\mu\text{m}/\text{m}$, about 10% higher (Fig. 10).

During the test T2, several shear reinforcements near the edge of impact surface have been found broken due to the important percussion force. The calculated maximum plastic strain in shear reinforcement is 11.4‰, from which we can consider that the stirrups are broken. Namely, stirrups can be considered as strongly anchored: with a 10‰ plastic deformation, their extension should be about 2 mm, which is far beyond their extension capacity within the slab thickness during impact. These numerical results show that, during impact, the high stress in concrete is relatively concentrated in the impact zone and the risk of shear failure due to yielding of stirrups is correctly anticipated in this impact analysis.

The directions of the principal plastic extension of concrete and the experimental crack pattern during the test T1 are shown in Fig. 11. The former suggests the orientation of cracks, which should be perpendicular to these extensions. By comparison, a correct qualitative agreement can be admitted. Moreover, crack openings can be estimated from integration of the plastic strain in the reinforcements over their anchor length ($W_{\text{max}}=2* \varepsilon_{\text{max}}^p *l$). The maximum plastic strain of flexural reinforcement is about 2.5‰ in the test T1, the anchor length is taken as $l=0.07$ m (half of bars spacing), corresponding to about 0.35 mm opened cracks, which seems of the same order of amplitude as observed.

A detailed comparison of the structural local results is given in Table 7.

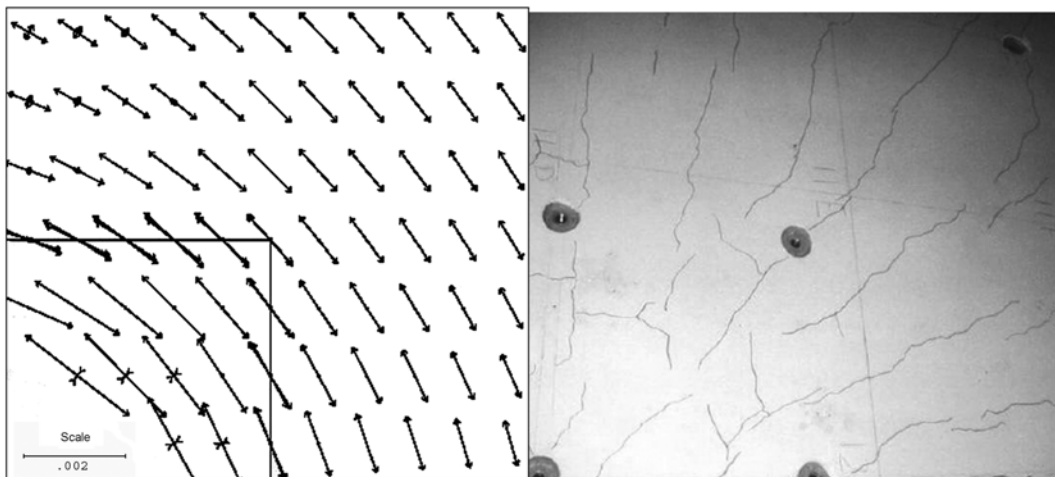


Fig. 11 Principal plastic extension directions and experimental crack pattern in intrados of impact zone (T1: 1.5 m×1.5 m) (Delhomme *et al.* 2005)

Table 7. Structural local results

Impact test	Concrete		Steel bars	
	Experimental results	Numerical results	Experimental results	Numerical results
T1	Few cracks in the Zone 1	Crack opening width: $W_{\max} = 0.35$ mm	No steel bars yielding	Steel bars yielding in the Zone 1 ($\varepsilon_{\max}^p = 3\%$ for shear bars and 2.5% for flexural bars)
T2	Important cracks in the Zone 2	Crack opening width: $W_{\max} = 0.56$ mm	5 shear bars (HA8) broken in the Zone 2	Steel bars yielding in the Zone 2 ($\varepsilon_{\max}^p = 11\%$ for shear bars and 4% for flexural bars)
T3	Very few cracks in the Zone 3	Non comparable results	No steel bars yielding	Non comparable results for the beam element fuse supports modelling
T4	Few cracks in the Zone 2	Crack opening width: $W_{\max} = 0.56$ mm	No steel bars yielding	Flexural bars yielding in the Zone 2 ($\varepsilon_{\max}^p = 4\%$)
T5	Important cracks in the Zone 1	Crack opening width: $W_{\max} = 0.70$ mm	Steel bars yielding in the Zone 1	Steel bars yielding in the Zone 1 ($\varepsilon_{\max}^p = 12\%$ for shear bars and 5% for flexural bars)
T6	Concrete ejection in the Zone 2	Crack opening width: $W_{\max} = 1.40$ mm	Several shear bars (HA10) broken in the Zone 2	Steel bars yielding in the Zone 2 ($\varepsilon_{\max}^p = 21\%$ for shear bars and 10% for flexural bars)

3.5. Numerical simulation assessment

The object of the proposed impact analyses is not to reproduce exactly the experimental procedures and results, as carried out e.g. in (Berthet-Rambaud *et al.* 2003). Here, the aim consists in developing an appropriate impact algorithm to analyze SDR structure under rock-fall impacts and find out the ultimate limit states for SDR structure design. This impact analysis needs to allow checking the adjustment of the numerical results close to the experimental ones with a possible engineering safety margin, and validating the sensitivity of the numerical results to relevant engineering factors and input data. In spite of the simplified finite element modelling hypotheses (spherical rigid block and neglected frictions), the numerical results are able to reasonably predict the SDR structural response and sensitivity under rock-fall impacts. By using this kind of impact analysis, we can:

- Determine the input data without ambiguity: the material properties used for computations can be determined directly from experiments and have physical meanings (Tables 2, 3 and 4);
- Calculate impact force (amplitude, duration, impulsion) with an acceptable safety margin over its maximum value: the numerical impact force or impulsion (one impact) is conservative with respect to the combination of the experimental forces or impulsions (possible rebound) (Table 5);
- Anticipate the global flexural behaviour of SDR structure: the numerical maximum vertical displacement of R.C. slab is about 11%~18% higher than the experimental one (Table 6);
- Anticipate the yielding of fuse supports: the fuse supports yielding is detected by their numerically estimated significant irreversible displacement (Table 6);
- Anticipate the yielding of steel shear and flexural reinforcements: the steel reinforcements yielding is estimated through their plastic strain (Table 7);

- Anticipate the direction of cracks in concrete and have a rough estimate of cracks opening: the direction of cracks and their opening width are estimated by the direction of principal plastic extensions of concrete and the maximum plastic strain of steel reinforcements (Table 7);
- Distinguish the different impacting energy levels (SLS, ULS and PULS) by the stresses and strains in reinforcing bars and concrete (Table 7).

4. Structural design: sensitivity study with respect to the impact location

4.1. Impact location and impact analysis model

In order to quantify the influence of rock block impact location on the SDR structure behaviour and to precise the SDR structure design procedure in correctly anticipating the critical impact point locations, a series of impact analyses have been carried out on this 1/3 scaled SDR structure (same as experimentally tested by Delhomme *et al.* 2005) corresponding to 10 different impact points, as illustrated in Fig. 12. These impact points have been chosen in a quarter of the slab due to the structure axial symmetry. A block of 450 kg dropped from 30 m impacts independently in these 10 points. The impact energy is 135 kJ, corresponding to the ULS impact energy level.

4.2. Numerical results

The results of impact force maximum values are listed in Table 8. They are found to vary slightly with respect to the impact point position. The maximum value is about 5 MN, the contact duration is about 5 ms, and impulsions vary between 11.6 and 13.3 kN.s. Among these limited variations, the impact forces when the impact is located at the slab mid-span and upon the fuse supports points are higher than those in the intermediate positions. When the impact is located upon the fuse supports points, the force transmission to fuse supports produces a higher impact force, but the impulsion is lower due to the shorter impact duration. In a conservative design approach, this maximum impact force, determined from an impact analysis at the slab centre, can be used all over the slab area for verification with respect to the slab punching shear.

The numerical results of slab maximum vertical displacement are also detailed in Table 8. The

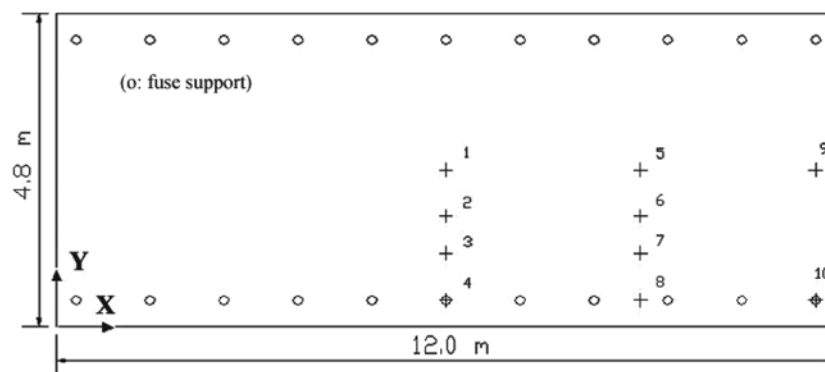


Fig. 12 Impact locations

Table 8. Numerical results of impact force and vertical displacement

Impact locations	Impact force amplitude (MN)	Impact duration (ms)	Impulsion (kN.s)	Maximum vertical displacement (mm)
1	5.6	5.1	13.3	26.0
2	5.1	5.0	12.6	22.5
3	5.1	5.5	12.6	20.1
4	5.6	5.1	11.9	22.3
5	5.3	5.5	13.2	25.0
6	5.1	5.0	12.5	22.3
7	5.1	5.5	12.5	19.7
8	5.5	5.8	11.9	21.1
9	5.5	6.1	11.8	50.5
10	5.4	5.0	11.6	35.2

slab deforms most when the impact is located in the centre or in the mid-span of slab, this means that the slab centre is the critical position for slab flexural reinforcements design, which remains consistent with the quasi-static flexural design in the slab centre in the conventional design method. The numerical results show that the maximum plastic strain of flexural steel reinforcements under the 135 kJ impact in location 1 is 4.4%, which indicates that the flexural reinforcements are sufficiently designed for ensuring ULS bending strength verification with a satisfactory safety margin.

This impact position sensitivity study has also quantitatively emphasized an edge effect of the SDR structure. When impacts take place at the edge of the structure, slab and fuse supports displacements have almost been doubled (locations 9 and 10 in Table 8) due to the reduced structure rigidity and fuse supports number on the edge. This should be taken into account in the structure design by adopting methods such as augmentation of the section height, local stiffness enhancement by additional reinforcing bars or beams and increase of the fuse supports section.

Moreover, no matter where the impact point is, the numerical results show that the flexural reinforcements in the impact zone have locally yielded. And the 8 mm diameter shear reinforcements in the intense shear stress zone can be considered as broken since their plastic strain is superior to 10%. So, under the ULS energy level impact (rigid impact block: $m=450$ kg, $V=24.5$ m/s, $r=0.36$ m), wherever the impact location, we can consider that the stirrups on the edge of the zone (0.5 m* 0.5 m) near the impact point have been broken (45° cracks diffusion angle), and concrete in the zone (1.3 m* 1.3 m) near the impact point has been severely damaged.

4.3. Concluding remarks on the choice of impact location for design

This impact location sensitivity study has shown that the centre of slab can be considered as the critical impact position for the slab bending strength and punching shear resistance design. As for the fuse supports design, the fuse supports points can be considered as the critical impact position. Furthermore, in order to avoid frequent repair of fuse supports, they need to be able to resist the same ULS energy level when impact is at the slab centre. At the edge of SDR structure, particular design considerations should be taken to improve structure local rigidity and inertia.

Either for slab bending strength and punching shear resistance verification, or for fuse supports

bearing capacity, a critical design force level should be consistently chosen, in the sense of the limit of reversible behaviour, and of the limit of admissible repair. In both cases, these limits should be related to the statistics of rock-fall impacts, and to the desired return period of minor/major repair operations.

5. Structural design: sensitivity study with respect to the impact characteristics

5.1. Finite element model for the analyses

In the following SDR structural design studies, the impact has been positioned at the slab centre. In order to optimize SDR structural concept, especially its punching resistance design, SDR structural responses have been considered under different impacts with respect to the design load characteristics (rock block mass, velocity and radius) and different engineering parameters choices (slab concrete type, thickness and rigidity of a thin protective overlay, reinforcement ratio in the slab).

Due to structure axial symmetry, only a quarter of the 1/3 scaled SDR has been modelled. The finite element model and the input data for material properties and calculation parameters are the same as those in §3.2. The stiffness of fuse supports and neoprene layer in symmetrical plans is reduced to a half and nodes belonging to symmetrical plans are blocked in the perpendicular direction. In the case of a protective overlay, it is modelled as a solid volume, and its contact with the slab is considered as perfect. Altogether, the finite element mesh consists of about 5600 8-noded volume elements and about 6000 2-noded beam elements.

5.2. Initial impact energy effect (block mass and velocity)

Simplified protective structures design considers that the structural response depends directly on the incident kinetic energy of block, or on the impulsion given to the structure. Limits of this simplification were investigated by considering three different block masses: 200, 450, 810 kg and three different incident velocities: 17.3, 24.5, 27.2 m/s. These calculations also allow better understanding the limits of reversible behaviour and admissible repair of the SDR structure. The representative numerical results are presented in Table 9.

Table 9. Numerical results of initial impact energy effect

Mass (kg)/Velocity (m/s)/Energy(kJ)	Impact force amplitude (MN)	Impact duration (ms)	Impulsion (kN.s)	Maximum vertical displacement (mm)	ε_{\max}^p (shear bars)	ε_{\max}^p (flexural bars)
200/17.3/30	3.5	2.2	2.4	8	0.0000	0.0000
200/24.5/60	5.4	2.4	6.0	12	0.0034	0.0020
200/27.2/74	5.7	2.6	6.7	14	0.0039	0.0024
450/17.3/67	4.8	3.9	9.1	17	0.0032	0.0025
450/24.5/135	5.8	4.9	13.1	26	0.0114	0.0044
810/17.3/121	5.0	6.4	15.9	30	0.0092	0.0046
810/27.2/300	6.5	14.0	24.8	58	0.0208	0.0100

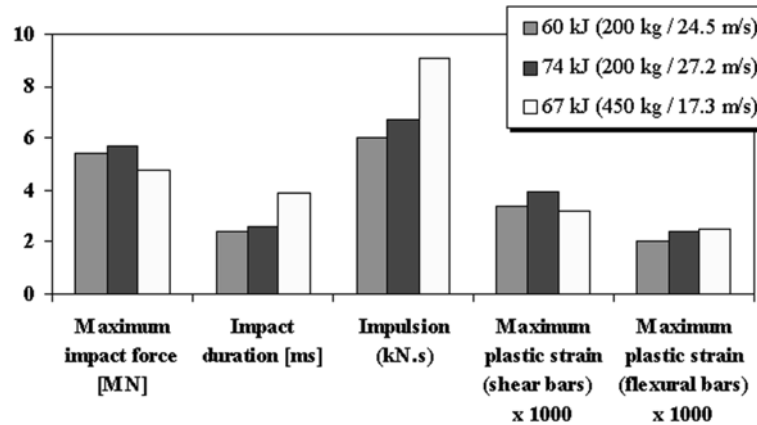


Fig. 13 Comparison of results of different initial impact energies

It is found that the maximum impact force, the impact duration and the impact impulsion increase roughly with the increasing impact energy. The maximum vertical displacement and the plastic strain of flexural reinforcement increase also with an increasing impact energy. However, their increases are neither proportional to the incident energy, nor to the impulsion. Moreover, the plastic strain of shear reinforcement (the punching failure risk) is directly associated with the impact force and its distribution. This is confirmed by comparing three impacts with respect to the maximum impact force, the impact duration, the impulsion and the maximum plastic strains of steel reinforcement, as illustrated in Fig. 13. These three impacts are roughly similar in terms of incident energy (60, 74 and 67 kJ), but with different masses and velocities (200 kg/24.5 m/s; 200 kg/27.2 m/s; 450 kg/17.3 m/s).

It turns out that even with a lower incident energy and impact force, a heavier block may cause more severe flexural damage due to its longer impact duration, which leads to larger impulsion. However, the higher plastic shear strains in shear bars are obtained with the higher block velocity (the maximum impact force). For the intense impacts leading to nonlinear structural response, it is thus demonstrated that neither the maximum impact force, nor the impact energy or the impact impulsion can be the only parameter to design SDR structure. A detailed analysis, taking into account the rock block-SDR structure interaction, remains necessary for ensuring its safe design verification. It is at the time when the impact force is maximum that concrete and reinforcement stresses should be verified, and at the time of maximum vertical displacement (about one quarter of the structure fundamental period) that the material plastic strains should be verified.

5.3. Block radius (local contact curvature)

With a similar attempt to define safe design conditions, a series of calculations have been carried out to study the influence of the block local contact curvature radius at the impact location. Five different radii have been taken into account: 0.36, 0.54, 0.72, 0.90, 1.08 m under the same 135 kJ impact ($m=450$ kg, $V=24.5$ m/s). The smaller radius corresponds to a spherical-shaped block with uniformly distributed mass.

The numerical results show that the block radius variation has an important effect on the maximum impact force, which has almost been doubled when the radius increases from 0.36 m to

1.08 m. Nevertheless, the impact duration decreases and the impact impulsion decreases slightly from 13.1 to 12.1 kN.s. The maximum vertical displacement is almost constant (about 26 mm), meaning that block radius variations have rather a local than a global effect on the structural response. Analyzing the maximum plastic concrete extensions shows that the larger impact force is distributed over a larger contact area, the maximum principal plastic tensile strain of concrete decreases from 0.104 to 0.043 when the radius augments from 0.36 to 1.08 m. At the same time, the maximum plastic strains of shear and flexural reinforcing bars also decrease slightly (from 11.4‰ to 10.5‰ and 4.4‰ to 4.0‰, respectively).

The critical block radius for design is thus demonstrated to be the smallest possible, and as a reference, the radius corresponding to a spherical block for a given impact block mass.

6. Structural design: influence of different engineering parameters

After having clarified what shall be considered as the impact design “load” with respect to the incident block description (mass, velocity and radius), the most critical issue for the SDR structural design remains ensuring its ability to resist possible punching failure during the short impact phase. In fact, punching shear appeared to be critical during the tests (Delhomme *et al.* 2005) for the impacts producing even limited flexural irreversible damage. The influence of possibly efficient parameters determined by the engineers such as concrete type, thickness and rigidity of a thin protective overlay and reinforcement ratio in the slab has thus been investigated for a 135 kJ impact ($m=450$ kg, $V=24.5$ m/s, $r=0.36$ m) (ULS energy level impact), so that efficient design choices can be oriented.

According to the results of the previous study, we focused on the impacts at the slab centre. Due to structure axial symmetry, only a quarter of structure has been modelled. The finite element model and the input data for material properties and calculation parameters are the same as those in §5.1.

6.1. Concrete type

In the initial concept of SDR structure as well as in the 1/3 scaled tests, 30 MPa-concrete was used. Variation of concrete properties was considered using experimental characterization of Fiber Reinforced Concrete (FRC) and High Performance Concrete (HPC) (Toutlemonde and Rossi 1995, Sercombe 1997). These data are not related to precisely optimized industrial choices, but should allow for the calculations with possible higher material resistance and/or stiffness.

The dynamic behaviour of FRC and HPC in the strain rate range from 10^{-6} to 10 s⁻¹ can be explained by the viscous effects due to the presence of liquid (free water) within the nanopores of concrete (Toutlemonde and Gary 2004). So, Sercombe’s model has been used to model FRC and

Table 10. FRC and (HPC) properties used for impact analyses

static elastic modulus (E)	42 (41) (GPa)
uniaxial compressive strength (σ_c)	56 (80) (MPa)
uniaxial tensile strength (σ_t)	4.8 (5.1) (MPa)
asymptotic dynamic modulus (E_{lim}^{dyn})	47.4 (45.2) (GPa)
absolute increase in tensile strength (α)	0.54 (0.75) (MPa/log. unit)

HPC behaviour under rock-fall impacts, main adaptations concern concrete properties, listed in Table 10.

For FRC, the experimental results show an increase of concrete tensile resistance equal to 0.54 MPa/log. unit. An average increase of 0.9 GPa/log. unit. has been considered over 6 logarithmic decades for the dynamic modulus evolution. Moreover, for FRC, its uniaxial tensile strength σ_t is an equivalent plastic stress (Chanvillard 2000), defined for a maximum crack opening of 0.5 mm (which corresponds to the crack opening in the tensile tests of notched samples) (Sercombe 1997). Through this equivalent plastic stress, the post-cracking behaviour of fiber reinforced concrete and the related rate effects can be easily introduced in this finite element impact analysis.

For HPC, the experimental results show an increase of concrete tensile resistance equal to 0.75 MPa/log. unit. An average increase of 0.7 GPa/log. unit. has been considered over 6 logarithmic

Table 11. Numerical results with different concrete types

Concrete type	Impact force amplitude (MN)	Impact duration (ms)	Impulsion (kN.s)	Maximum vertical displacement (mm)	ϵ_{max}^p (shear bars)	ϵ_{max}^p (flexural bars)
C	5.8	4.9	13.1	26	0.0114	0.0044
FRC	7.3	4.1	13.2	23	0.0089	0.0041
HPC	8.3	3.7	13.4	21	0.0076	0.0041

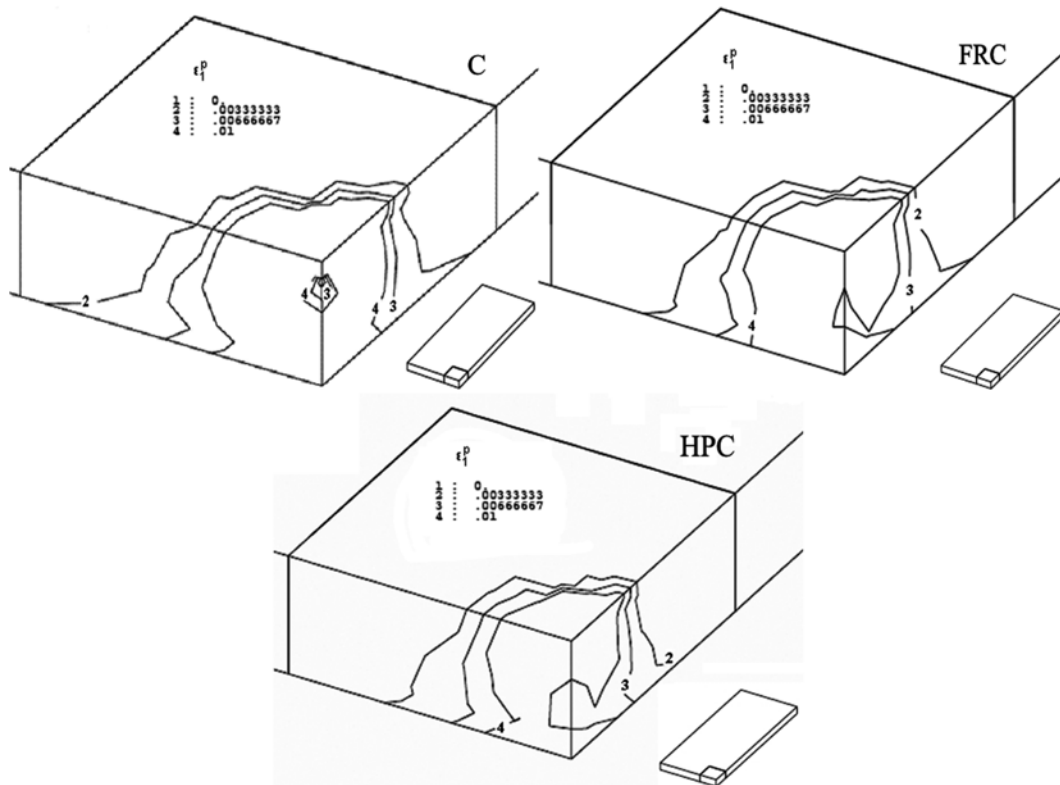


Fig 14 Comparison of the damaged zone in the slab with three concrete types for slab: C, FRC and HPC (Concrete principal plastic tensile strain ϵ_1^p : 1: 0; 2: 0.0033; 3: 0.0067; 4: 0.01)

decades for the dynamic modulus evolution.

The representative numerical results are presented in Table 11, which show that the maximum impact force increases with an increasing concrete resistance and modulus, and impulsion increases slightly. However, impact duration and the maximum vertical displacement decrease. Moreover, the distribution of concrete plastic extensions shows that the size of the severely damaged zone is reduced in the case of FRC and HPC because of the higher resistance of the material (Fig. 14). The maximum plastic strains of shear and flexural reinforcing bars decrease from 11.4‰ to 7.6‰ and 4.4‰ to 4.1‰ respectively. The higher concrete contribution to shear resistance of HPC may explain this significant decrease in shear reinforcement plastic strain (Toutlemonde and Rossi 1996).

So, under the same impact energy, a more resistant concrete material can improve the structural global behaviour by decreasing the vertical displacement, and also the structural local behaviour by restricting the damaged zone and decreasing the plastic strain of steel bars.

6.2. Protective overlay thickness and rigidity

Even under relatively weak impact energy with respect to the flexion, the slab should resist locally an important impact force. To better resist this impact force and avoid the slab punching failure, a protective overlay is often used (Mikami *et al.* 1995). A thin protective overlay has thus been taken into account here to improve the local dissipation. This overlay is not to dissipate the whole impact energy, therefore its thickness is limited to several centimeters to avoid increasing too much the structural permanent weight. This thin overlay can be damaged under violent impacts to protect the slab, the majority of impact energy will still be dissipated by the slab movement and deformation.

The thickness and rigidity of this overlay have been studied consequently. At first, thicknesses of 0, 2, 4 and 6 cm in 1/3 scaled have been studied for an overlay made of conventional concrete. Then, the influence of overlay concrete type has been studied with a 4 cm thickness. Three different concrete materials have been considered for this overlay: Concrete, FRC and HPC. Their properties are the same as those in the previous studies.

The representative numerical results are given in Table 12. If we take the slab without overlay as reference, we find that this thin protective overlay helps decreasing slab vertical displacement due to its contribution to the structural global rigidity. The maximum impact force increases with an increasing overlay thickness, impact duration decreases, and impact impulsion increases slightly.

Table 12. Numerical results of protective overlay thickness and rigidity

		Impact force amplitude (MN)	Impact duration (ms)	Impulsion (kN.s)	Maximum vertical displacement (mm)	ε_{\max}^p (shear bars)	ε_{\max}^p (flexural bars)
Overlay thickness	e=0 cm	5.8	4.9	13.1	26	0.0114	0.0044
	e=2 cm	5.9	4.8	13.5	24	0.0111	0.0043
	e=4 cm	6.4	4.7	13.6	22	0.0098	0.0039
	e=6 cm	7.0	4.3	13.8	16	0.0085	0.0036
Overlay rigidity (e=4 cm)	C	6.4	4.7	13.6	22	0.0098	0.0039
	FRC	7.2	3.9	14.0	20	0.0097	0.0038
	HPC	8.0	3.8	14.0	20	0.0096	0.0036

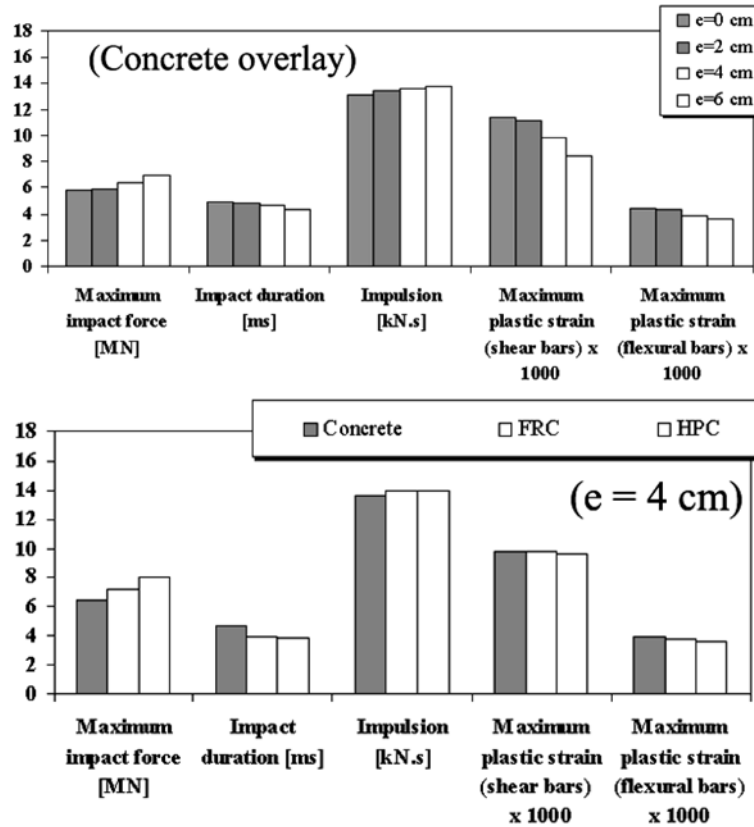


Fig. 15 Comparison of plastic strains within reinforcing bars with different overlay thicknesses and rigidities

The concrete plastic extensions decrease with an increasing overlay thickness, also for the plastic strain of steel bars (Fig. 15). If we take the slab with a concrete overlay as reference, we find that a more rigid overlay (FRC and HPC) can better distribute the impact force, even if this force has a higher value. And the overlay geometrical diffusion effect appears to be more efficient than its rigidity increase, both for limitation of concrete plastic extensions and for limiting plastic strains of steel bars (Fig. 15). These results confirm the protective function of overlay.

6.3. Reinforcement ratio in the slab

Varying slightly the reinforcement ratio in the slab allows checking the efficiency of design variations. Here, the reference test is the concrete slab without overlay under a 135 kJ impact ($m=450$ kg, $V=24.5$ m/s, $r=0.36$ m ULS energy level impact), the diameter of shear and flexural reinforcing bars has been altered by a 2 mm-increase and reduction. Notations are as follows: FB-: flexural bars diameter-2 mm; FB+: flexural bars diameter+2 mm; SB-: shear bars diameter-2 mm; SB+: shear bars diameter+2 mm.

The representative numerical results are presented in Table 13, which show that these variations turn out to have little influence on the maximum impact force, impact duration, impact impulsion and the maximum deflection. Yet, they have a significant influence on the reinforcements strains. In

Table 13. Numerical results of reinforcement ratio variations

Reinforcement section variations	Impact force amplitude (MN)	Impact duration (ms)	Impulsion (kN.s)	Maximum vertical displacement (mm)	ε_{\max}^p (shear bars)	ε_{\max}^p (flexural bars)
FB-	5.7	4.9	13.0	27	0.0121	0.0059
FB+	5.8	4.9	13.1	26	0.0105	0.0021
SB-	5.7	4.9	13.0	26	0.0199	0.0047
SB+	5.8	4.9	13.0	26	0.0000	0.0043
Reference test	5.8	4.9	13.1	26	0.0114	0.0044

fact, the variations of reinforcement ratio in the slab are of little influence on the slab local rigidity in the impact zone. However, different sections of reinforcing bars can take different forces. The numerical results show that the increase of shear reinforcements ratio can possibly prevent SDR structure from punching failure, since the maximum plastic strain in shear reinforcement may be decreased from 10‰ to 0‰.

7. Conclusions

This paper deals with Three-Dimensional finite element rock-fall impact analyses of a reinforced concrete SDR structure. A proper impact algorithm has firstly been presented, aiming to simulate SDR structure behaviour with simplified finite element modelling hypotheses to find out the ultimate limit states for its design. The numerical results correctly approximate the experimental results, which support the efficiency and robustness of this new SDR structural concept. Even if they do not precisely represent details of the interaction (like bloc deformability, rebound, frictions), they prove to be reasonably sensitive to the different parameters, which is useful for the designer when anticipating the effects of design assumptions and variations.

Then, by using this validated numerical tool, finite element impact analyses have been carried out to determine the most critical impact location. The numerical results have confirmed that the slab centre is the critical position for slab design, while for fuse supports design, it is the fuse support point. Moreover, particular design considerations should be taken to improve the structure rigidity and inertia at the edge.

Furthermore, impact analyses have then been carried out at the slab centre with variations of characteristics of incident impact block. Due to the independent influence of block mass and velocity, it is demonstrated that an impact analysis remains necessary to account for the interaction between block/SDR structure. For a critical impact level derived from the tests (limit of punching shear), a safe design situation is found with a reference block radius considered as a homogeneous sphere.

Finally, trying to reduce the risk of slab punching shear failure, several series of parametric analyses have also been carried out with impact at the slab centre, with respect to the engineered characteristics of the SDR structure. It is shown that using high performance concrete for the slab and increasing the shear reinforcement ratio in the slab are the most efficient methods to prevent slab punching failure. Moreover, a thin rigid protective overlay can limit concrete damage and increase slab punching resistance.

All these numerical simulations demonstrate the predictive capacities of the developed numerical tool, even with simplified finite element modelling hypotheses. This tool helps to quantify the different design solutions of SDR structure and can be enriched to study other similar impact problems.

Acknowledgements

The authors are indebted to Pierre Humbert, Head of the Department for Numerical Models at LCPC, for assisting the implementation of the impact algorithm in CESAR-LCPC. The authors also sincerely thank Pascal Perrotin, Professor at ESIGEC in Université de Savoie and Jean Tonello, inventor of the SDR structure, working for Tonello I.C., for communication of the experimental results and photos of the tests, as well as Philippe Bisch, Professor at Ecole Nationale des Ponts et Chaussées, for his advice about this article.

References

- Berthet-Rambaud, P. *et al.* (2003), "Structural modelling of reinforced concrete slabs subjected to falling rock impacts", *Proceeding of Euro-C 2003 Conference*, A.A Balkema Publishers, 599-604.
- CEB (1988), *Concrete structures under impact and impulsive loading (synthesis report)*, Bulletin d'information, **187**.
- Chanvillard, G. (2000), "Characterisation of fibre reinforced concrete mechanical properties: a review", *BEFIB'2000*, RILEM Proceedings PRO15, 29-49.
- Coussy, O. (1995), *Mechanics of porous continua*, John Wiley & Sons, Chichester, England.
- Delhomme, F. *et al.* (2005), "Behaviour of a structurally dissipating rock-shed: experimental analysis and study of punching effects", *Int. J. Solids Struct.*, **42**, 4204-4219.
- Harsh, S. *et al.* (1990), "Strain-rate sensitive behaviour of cement paste and mortar in compression", *ACI Mater. J.*, **87**(5), 508-516.
- Humbert, P. *et al.* (2005), "CESAR-LCPC: A computation software package dedicated to civil engineering uses", *Bulletin des Laboratoires des Ponts et Chaussées*, **256-257**, 7-37.
- IVOR (2001), *Label IVOR : Couverture pare-blocs structurellement dissipante*, Direction de la Recherche et des Affaires Scientifiques et Techniques, Ministère de l'Équipement, des Transports et du Logement, France (French government innovation label).
- Lussou, P. and Toutlemonde, F. (2005), "F.E.-aided optimization of energy dissipation in a new type of rock-sheds", *3rd International conference on Construction Materials : Performance, innovations and structural implications, CONMAT'05*, Vancouver, 2005, Proc. ed. by N. Banthia *et al.*, theme 1, chapter 12 Seismic Loading, Fatigue Loading, Impact Loading, and Blast Loading, 8 pp, abstract, 167.
- Lussou, P. *et al.* (2005), "Modélisation du béton en dynamique rapide avec le module MCCI de CESAR-LCPC", *Bulletin des laboratoires des Ponts et Chaussées*, Numéro spécial CESAR-LCPC, **256-257**, juillet-août-septembre, 215-226.
- Mikami, H. *et al.* (1995), "Shock absorbing performance of a three-layered cushion system using RC core slab reinforced with AFRP rods", *Concrete under Severe Conditions*, E&FN Spon, 1633-1643.
- OFR (1998), Office fédéral des routes, Direction des travaux CFF, *Actions sur les galeries de protection contre les chutes de pierres : directive*, Berne, Suisse.
- Rossi, P. (1997), "Strain rate effects in concrete structures: the LCPC experience", *Materials and Structures*, (Hors série-Report of the RILEM 50th General Council), **100**, 54-62.
- Sercombe, J. (1997), *Modélisation du comportement du béton en dynamique rapide : application au calcul des conteneurs à haute intégrité*, Ph.D. Thesis, Ecole Nationale des Ponts et Chaussées, France.

- Sercombe, J. *et al.* (1998), "Viscous hardening plasticity for concrete under high rate dynamic loading", *J. Eng. Mech.*, **124**(9), 1050-1057.
- Toutlemonde, F. and Rossi, P. (1995), "Major parameters governing concrete dynamic behaviour and dynamic failure of concrete structures", *DYMAT J.*, **2**(1), 69-77.
- Toutlemonde, F. and Rossi, P. (1996), "Are high-performance concretes (HPC) suitable in case of high rate dynamic loading?", *the 4th International Symposium on Utilization of High-Strength/High-Performance Concrete*, Presses de l'ENPC, Paris, 695-704.
- Toutlemonde, F. *et al.* (1999), "Développement d'un conteneur pour l'entreposage de déchets nucléaires : résistance au choc", *Revue Française de Génie Civil*, **3**(7-8), 729-756.
- Toutlemonde, F. and Gary, G. (2004), *Comportement dynamique des bétons et génie parasismique* (Editeurs: J. MAZARS, A. MILLARD) - chapitre 1. *Comportement dynamique du béton : aspects expérimentaux*, Lavoisier, Hermès Science ISBN 2-7462-0879-2, 21-76.
- Ulm, F.-J. and Coussy, O. (2001), "Some time and lengths scales in durability mechanics of concrete structures", *Concrete Sci. Eng.*, **3**(11), 121-134.
- Zhang, Y. (2006), *Analysis and design of protective structures against rock falls*, Ph.D. Thesis, Ecole Nationale des Ponts et Chaussées, France. (In French)